Reconstructing Network Dynamics of Coupled Discrete Chaotic Units from Data

Irem Topal* and Deniz Eroglu†
Faculty of Engineering and Natural Sciences, Kadir Has University, 34083 Istanbul, Turkey

(Received 20 September 2022; revised 17 February 2023; accepted 21 February 2023; published 15 March 2023)

Reconstructing network dynamics from data is crucial for predicting the changes in the dynamics of complex systems such as neuron networks; however, previous research has shown that the reconstruction is possible under strong constraints such as the need for lengthy data or small system size. Here, we present a recovery scheme blending theoretical model reduction and sparse recovery to identify the governing equations and the interactions of weakly coupled chaotic maps on complex networks, easing unrealistic constraints for real-world applications. Learning dynamics and connectivity lead to detecting critical transitions for parameter changes. We apply our technique to realistic neuronal systems with and without noise on a real mouse neocortex and artificial networks.

DOI: 10.1103/PhysRevLett.130.117401

Dynamical networks, including power grids, food webs, climate networks, and neuron networks described by dynamical units oscillating on complex networks, are fundamental components of our everyday lives. The ability to regulate network dynamics is crucial for predicting, thus, controlling these systems' behavior to acquire the desired functionality. Neuron networks are an important class of dynamical networks for human wellness since the changes in the interaction can lead to undesired pathological situations. For instance, epileptic seizures are associated with emergent neural network synchronization when the dynamical network parameters change [1]. Consequently, it is vital to anticipate critical transitions to neuronal synchronization and invent predictive technologies to detect early warning signals to prevent potential tragedies [2]. In the case of neuron network dynamics, consisting of intrinsic neuron function and the coupling scheme between neurons, the critical transitions to synchronization are not directly determinable. Therefore, the governing equation must be recovered from the observations of the nodes for forecasting the critical transitions due to parameter changes.

The network dynamics reconstruction from data is a very active research field [3–8]. Various methods were proposed to infer the connectivity matrix under some constraints, such as the need for a system to be at steady state [9] or requiring prior knowledge about the dynamics [10–12] or the coupling strength [13]. In addition to the studies that reveal the connectivity matrix by control signals or analytical solutions, statistical learning approaches such as compressed sensing were also introduced to learn entire unknown dynamics [14,15], which also infers the connectivity structure. However, statistical learning techniques are not extendable for large networks or require long time series measurements. A natural question is then whether revealing the network dynamics of weakly interacting chaotic oscillators would be possible using relatively short data without requiring knowledge of the system's nodal behavior and coupling scheme. This question is especially relevant in weak coupling regimes, in which the synchronization regime is unstable and the decay of correlation is exponential for chaotic oscillators, meaning that similarity measures cannot capture the interaction topology.

This Letter reports a dynamical network reconstruction approach from time series observations by integrating mean-field approaches from dynamical systems theory with statistical learning tools. Neural networks are described by chaotic isolated dynamics [16], weakly interacting nodes [17], and interaction through scale-free type networks [18]. Our reconstruction approach assumes that we have the mentioned neuroscientific setting and access to all nodes' data while the local dynamics of the nodes, the coupling function between them, and the interaction structure are unknowns. Our methodology accurately identifies them using rather short time series and is independent from the network size, which is important since it is, generally, impossible to have long real-world observations, and real networks are large. Finally, as the reconstruction methodology includes mean-field approximations, the inferred model may not estimate the exact future states of the system due to the chaotic nature of the dynamical units. However, the reconstructed model allows us to predict the emergent collective behavior of dynamical networks considering parameter change, which is crucial to avoid undesired behaviors for real-world applications such as epilepsy seizures.

Model.—The network dynamics of weakly coupled and identical n oscillators with interaction akin to diffusion is described by

$$\boldsymbol{x}_i(t+1) = \boldsymbol{f}[\boldsymbol{x}_i(t)] + \sum_{j=1}^{n} w_{ij}\boldsymbol{H}[\boldsymbol{x}_i(t), \boldsymbol{x}_j(t)] + \boldsymbol{\eta}_i(t), \quad (1)$$

where $\boldsymbol{x}_i \in \mathbb{R}^m$, $\boldsymbol{f}\colon \mathbb{R}^m \to \mathbb{R}^m$ represents the isolated dynamics of nodes, and we assume it is chaotic [19]. $\boldsymbol{H}$ is a diffusive coupling function [$\boldsymbol{H}(\boldsymbol{x},\boldsymbol{x}) = \boldsymbol{H}(0) = 0$ and $\boldsymbol{H}(\boldsymbol{x},\boldsymbol{y}) = -\boldsymbol{H}(\boldsymbol{y},\boldsymbol{x})$]. $\boldsymbol{W} = [w_{ij}] \in \mathbb{R}^{n\times n}$ is the adjacency matrix of weighted and directed network where $w_{ij} \geq 0$ is the interaction strength from node j to node i. The noise term, $\boldsymbol{\eta_i}(t)$, is uniformly distributed $\|\boldsymbol{\eta_i}(t)\| \leq \eta_0$ for all nodes where η_0 is noise intensity. This network dynamics, Eq. (1), is used to model numerous real-world applications including brain networks [20], power grids [21,22], superconductors [23], and cardiac pacemaker cells [24].

Reduction theorem.—A low-dimensional reduction of Eq. (1) is key for our network dynamics reconstruction approach. The reduction theorem applies a mean-field approach that relies on two main statements: (i) the statistical behavior of nodes' dynamics (frequency distribution of states) must be preserved and (ii) a large portion of nodes must be interacting with at least a few nodes in the network. These statements are satisfied with the given assumptions for the reduction theorem: *chaotic local dynamics* of expanding maps and *weak coupling* (to preserve the nodes' state distribution against fluctuations due to the interactions or external noise) and *scale-free networks* (most of the nodes have small degrees $k \sim n^{\epsilon}$, and some nodes are hubs with degrees $k \sim n^{\frac{1}{2}+\epsilon}$ where ϵ is an arbitrarily small number), which also mimic brain network dynamics. Using the theorem, the coupling term of Eq. (1) can be reduced as follows:

$$\sum_{j=1}^{n} w_{ij}\boldsymbol{H}(\boldsymbol{x}_i,\boldsymbol{x}_j) \approx k_i \int \alpha\tilde{\boldsymbol{H}}(\boldsymbol{x}_i,\boldsymbol{x}_j)d\mu(\boldsymbol{x}_j)$$
$$= k_i\alpha(\tilde{\boldsymbol{V}}(\boldsymbol{x}_i) + \tilde{C}) = k_i\boldsymbol{V}(\boldsymbol{x}_i) + C,$$

where $\boldsymbol{V}$ is the effective coupling function, $k_i = \sum_j w_{ij}$ is the incoming degree of node i, $\boldsymbol{H} = \alpha\tilde{\boldsymbol{H}}$, α is a multiplier for the coupling function, μ is a physical measure of the isolated dynamics, C is the integration constant, and the integral takes into account the cumulative effect of interactions on node i. As the coupling term is reduced as a function of an invariant measure μ, the reduction theorem works for a system in a steady state. Furthermore, to apply this mean-field approach-based reduction theorem, the statistical properties of individual dynamical systems must be preserved, which is satisfied by chaotic oscillators and weak coupling (see Supplemental Material [25], Sec. II, and Ref. [32]). Then Eq. (1) can be written as

$$\boldsymbol{x}_i(t+1) = \boldsymbol{f}[\boldsymbol{x}_i(t)] + k_i\boldsymbol{V}[\boldsymbol{x}_i(t)] + C + \boldsymbol{\kappa}_i(t) + \boldsymbol{\eta}_i(t), \qquad (2)$$

where $\boldsymbol{\kappa_i}(t)$ is a small fluctuation for an interval of time that is exponentially large and depends on the state of neighbors of the ith node.

Reconstruction scheme.—To learn isolated dynamics $\boldsymbol{f}$ and coupling function $\boldsymbol{H}$, we first need to classify nodes regarding their degrees. According to the reduction theorem, nodes with a similar in-degree must have a similar governing equation. To identify the governing equations of each node independently from other nodes, we use sparse regression, particularly the sparse identification of nonlinear dynamical systems technique [33]. We denote the data collection of node i by Eq. (1) as $\mathcal{X}_i = [\boldsymbol{x}_i(1),\ldots,\boldsymbol{x}_i(T-1)]^T$ and $\mathcal{X}'_i = [\boldsymbol{x}_i(2),\ldots,\boldsymbol{x}_i(T)]^T$. The sparse identification of nonlinear dynamical systems technique performs a sparse regression for the linear equation $\mathcal{X}'_i = \boldsymbol{\Psi}(\mathcal{X}_i)\boldsymbol{\Xi_i}$ to solve for $\boldsymbol{\Xi_i} = [\xi_i^1,\ldots,\xi_i^p]^T$, which is a vector of coefficients that defines the dynamics, where $\boldsymbol{\Psi} = [\psi_1,\ldots,\psi_p]$ represents a library of basis functions and is applied to $\boldsymbol{x}_i$ as

$$\boldsymbol{\Psi}(\mathcal{X}_i) = \overbrace{\begin{bmatrix} \psi_1[\boldsymbol{x}_i(1)] & \psi_2[\boldsymbol{x}_i(1)] & \ldots & \psi_p[\boldsymbol{x}_i(1)] \\ \psi_1[\boldsymbol{x}_i(2)] & \psi_2[\boldsymbol{x}_i(2)] & \ldots & \psi_p[\boldsymbol{x}_i(2)] \\ \vdots & \vdots & \ddots & \vdots \\ \psi_1[\boldsymbol{x}_i(T-1)] & \psi_2[\boldsymbol{x}_i(T-1)] & \ldots & \psi_p[\boldsymbol{x}_i(T-1)] \end{bmatrix}}^{\text{candidate functions of } \boldsymbol{x}} \Big\downarrow \text{time}$$

where p is the number of candidate functions in the library $\boldsymbol{\Psi}$. (For a detailed description for the basis library, see Supplemental Material [25], Sec. VIII.) Sparse regression's goal is to determine the dynamics with a small number of functions in $\boldsymbol{\Psi}$ by finding active coefficients in $\boldsymbol{\Xi_i}$ (see Supplemental Material [25], Sec. VII). Consequently, we obtain a predicted model for each node only using the associated node's own data, and we expect to learn similar models for the nodes with similar in-degree k_i. A distance matrix is obtained by normalized Euclidean distance to classify the predicted models $d_{ij} = (\Sigma_{k=1}^{p}(1/V_k)|\xi_i^k - \xi_j^k|^2)^{1/2}$, where $|\cdot|$ is absolute value, V_k is the variance of the predicted coefficients of the kth function in $\boldsymbol{\Psi}$. Assume $\boldsymbol{\Xi_i}$ and $\boldsymbol{\Xi_j}$ are two predicted models of nodes i and j, which are presented as a linear combination of some functions within the library $\boldsymbol{\Psi}$. We get smaller d_{ij} for a similar pair of nodes i and j, while d_{ij} will be large for distinct nodes, such as a low-degree node and a hub. An example computation of d_{ij} can be found in Supplemental Material [25], Sec. VIII. The histogram $P(D)$ is obtained by the row sum of the distance matrix $D_i = \sum_j d_{ij}$, which provides an excellent classification for model similarities in terms of their degrees [Fig. 1(a)]. The low-degree nodes are expected to be located in the highest bin of the histogram since the network has many low-degree nodes. The models recovered for low-degree nodes are determined as our $\boldsymbol{f}$ with a negligible fluctuation $\boldsymbol{\kappa_i}$. Contrarily, the distance D_i is expected to be large for the hub nodes as they are the rarest. Therefore, hubs are located in the lowest bin of the histogram $P(D)$ [Fig. 1(a)]. Note that the success of the reconstruction depends on the separability of the low-degree nodes and hubs with respect to their degrees, which means the network topology plays

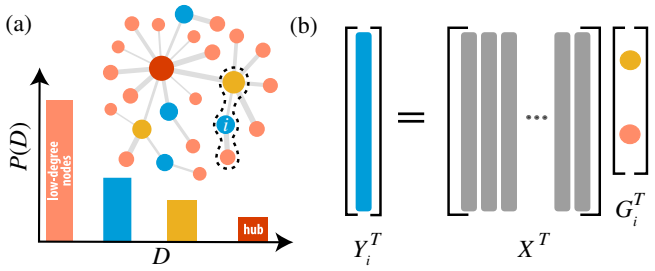

FIG. 1. Illustration of the reconstruction scheme. (a) Performing sparse regression on each observation gives predicted models for each node. Nodes with the same in-degree are reconstructed with the same predicted models, which allow us to classify nodes concerning their in-degrees. As low-degree nodes are abundant and represent the isolated dynamics with a negligible noise, learning $\boldsymbol{f}$ is possible. Discarding the local dynamics, $\boldsymbol{f}$, from the hub's data gives the dominant coupling effect on the hub. Therefore, the coupling function $\boldsymbol{H}$ can be learned. (b) After learning $\boldsymbol{f}$ and $\boldsymbol{H}$, the problem is defined as a linear problem for each node by subtracting the local dynamics, which obtains the remaining interaction effect for each node. Sparse regression on the remaining interaction dynamics of node i where $i = 1, \ldots, n$ entirely reconstructs the dynamical networks. Nonzero $\boldsymbol{G}_i^T$ elements are the incoming connections for ith node (see Supplemental Material [25], Sec. II, for a step by step scheme).

an important role here [2], which is further illustrated in Supplemental Material [25], Sec. II.

We obtain the cumulative coupling effect on the hub by discarding learned isolated dynamics contribution from the identified hub node's data as $\mathcal{X}_h' - \boldsymbol{f}(\mathcal{X}_h)$ where h denotes the hub node. We fit a function to the cumulative coupling effect on the hub and learn the coupling function $\boldsymbol{H}$ with a possible linear shift due to the integration constant C (Supplemental Material [25], Sec. II). The size of the linear shift can be easily estimated using $\boldsymbol{H}(\boldsymbol{0}) = \boldsymbol{0}$. Inferring the interaction function is vital to reveal the network [34], and learning $\boldsymbol{H}$ from such reduced dynamics increases the feasibility of our approach. Introducing the Laplacian matrix, $\boldsymbol{L}$ with $L_{ij} = \delta_{ij} k_i - w_{ij}$ where δ_{ij} is the Kronecker delta ($\delta_{ii} = 1$ and $\delta_{ij} = 0$ if $i \neq j$) and assuming that $\boldsymbol{H}$ is a linear function, we can rewrite Eq. (1) in a compact form as

$$\boldsymbol{X}(t+1) = \boldsymbol{F}[\boldsymbol{X}(t)] - (\boldsymbol{L} \otimes \boldsymbol{H})[\boldsymbol{X}(t)], \tag{3}$$

where $\boldsymbol{X} = [\boldsymbol{x}_1, \ldots, \boldsymbol{x}_n]^T$, $\boldsymbol{F}(\boldsymbol{X}) = [\boldsymbol{f}(\boldsymbol{x}_1), \ldots, \boldsymbol{f}(\boldsymbol{x}_n)]^T$, and $\otimes$ is the Kronecker product (see Supplemental Material [25], Sec. I, for the derivation in terms of Laplacian matrix and [35]). Defining $\boldsymbol{Y}(t) = \boldsymbol{X}(t+1) - \boldsymbol{F}[\boldsymbol{X}(t)]$, Eq. (3) can be written as $\boldsymbol{Y} = \boldsymbol{G}\boldsymbol{X}$ where $\boldsymbol{G} = -(\boldsymbol{L} \otimes \boldsymbol{H})$. Finally, we complete the reconstruction by learning sparse matrix $\boldsymbol{G} \in \mathbb{R}^{mn \times mn}$, by solving the linear equation $\boldsymbol{Y}^T = \boldsymbol{X}^T \boldsymbol{G}^T$ using sparse regression, namely least absolute shrinkage and selection operator (LASSO) [36], as suggested in Ref. [37]. LASSO adds the ℓ_1 regularization penalty to the least-squares loss function to find the sparse coefficients (the links), and it is assessed as a compressed sensing approach [38]. Note that the linear equation can also be solved with ℓ_2 norm for long time series; however, as we are interested in short data (in the case of the length of the time series $T < mn$) the compressed sensing approach must be employed [38]. Consequently, we learn the connectivity matrices $\boldsymbol{G}$ and $\boldsymbol{L}$ as seen in Fig. 1(b). It is also important to note that learning the equations of all nodes by a single sparse regression without the reduction theorem is only possible for relatively small networks. The library extension, due to network size, causes a statistically correlated data matrix that quickly fails on reconstruction [39,40]. A detailed discussion can be found in Supplemental Material [25], Sec. XII.

Mouse neocortex reconstruction.—A weighted and directed neural network (987 nodes and 1536 edges), representing a mouse neocortex [41,42], is considered (Supplemental Material [25], Sec. IV). To mimic neurons, we used electrically coupled Rulkov maps akin to diffusion as

$$u_i(t+1) = \frac{\beta}{1 + u_i(t)^2} + v_i(t) - \sum_j L_{ij} u_j + \eta_i$$
$$v_i(t+1) = v_i(t) - \nu u_i(t) - \sigma,$$

where the fast variable u_i is the membrane potential and the slow variable v_i is the ion concentration variation [43]. The constant parameters $\beta = 4.1$ and $\nu = \sigma = 0.001$ are fixed for chaotic bursting dynamics [44].

Noise-free case.—Following the reconstruction scheme, the nodes are classified using the similarity histogram Fig. 2(a) for $\eta_0 = 0$, while the pairwise Pearson correlations do not show any information about the degrees [inset in Fig. 2(a)]. The difference between return maps of a low-degree node and the hub is illustrated in Fig. 2(b), and the comparison against an isolated node dynamics is given in Supplemental Material [25], Sec. V-A. Effective coupling $\boldsymbol{V}(\boldsymbol{x})$ is found approximately $[0.1(u+1), 0]$, meaning that α is 0.1 and the linear shift is 1 on u variable due to $\boldsymbol{H}(\boldsymbol{0}) = \boldsymbol{0}$ [Fig. 2(c)]. Finally, we learn the network topology by solving the linear equation $\boldsymbol{Y} = \boldsymbol{G}\boldsymbol{X}$ using the learned $\boldsymbol{f}$ and $\tilde{\boldsymbol{H}}$. We measure the reconstruction error using the fraction of the false negatives (positives) out of the positives (negatives), FNR (FPR). The FNR (FPR) equals 0 for perfect reconstruction (Supplemental Material [25], Sec. III). Here, we use the ground truth Laplacian matrix to assess the accuracy of the reconstruction. When the ground truth is not available, the learned model can be evaluated by the cross-validation techniques (Supplemental Material [25], Sec. XI). The reconstruction error is found to be almost zero for a data length larger than $T > 200$ [Fig. 2(d)]. Furthermore, a systematical evaluation of our approach according to penalty terms and time series lengths is

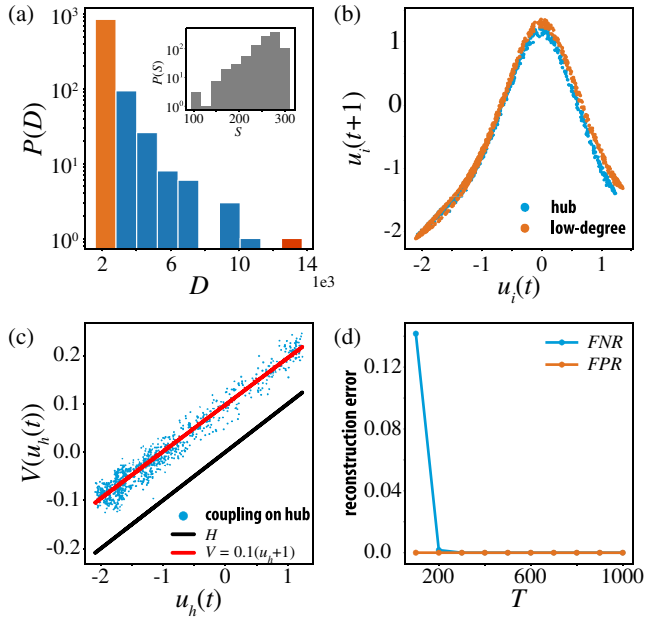

FIG. 2. Reconstruction procedure for weakly electrically coupled Rulkov maps on a real mouse neocortex network. (a) Node-similarity histogram determines the low-degree nodes (orange bar) and the hub (red bar). Inset: Histogram $P(S)$ presents the correlations between the original time series. It is impossible to infer the connectivity structure from the correlations due to the chaotic nature of the Rulkov maps. (b) The return maps of a low-degree node and the hub are slightly different due to weak coupling effect. (c) The effective coupling, $V(u)$, shifts through the horizontal direction due to the integral constant 1. (d) *FNR* for different lengths of time series. *FPR* are zero for all time series lengths.

performed. When the number of nodes n times the dimension of the local dynamics m exceeds the time series length $nm > T$, it corresponds to an underdetermined linear problem. Even for short data ($T \approx 200$), a successful reconstruction is possible with a small penalty term when $mn = 1974$ [Fig. 3(a)]. Note that if the problem is overdetermined $nm < T$, then ℓ_2-norm regression can be used for faster computations (Supplemental Material [25], Sec. IX). Furthermore, we provide reconstruction analysis for Hénon map and the Tinkerbell map in Supplemental Material [25], Sec. V. We also perform our procedure on a macaque monkey visual cortex network [42,45]. This network is not scale-free; however, assuming the local dynamics and the hub node are known, we reconstructed the network dynamics (see Supplemental Material [25], Sec. VI).

Noise effect on reconstruction performance.—To measure the robustness of our methodology against noise, we systematically perform the reconstruction procedure for various η_0 values [Eq. (1)] on synthetic as well as real mouse neocortex networks. The reconstruction approach is robust to small noise intensities for the real-world example [Fig. 3(b)]. The average robustness of the reconstruction procedure over 50 different directed and weighted random

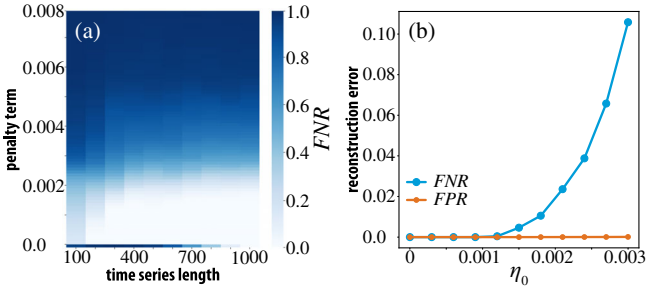

FIG. 3. (a) The reconstruction performance for different time series lengths and a series of penalty terms as *FNR*. *FPR* always equals 0 for this case. (b) Noise effect on reconstruction performance on real network as *FNR* and *FPR*.

scale-free networks is given in Fig. 4. The scale-free networks are generated using the algorithm in Ref. [46], and weights are assigned uniformly from the interval [0.8, 1.2]. The algorithm generates undesired self-loops and multiple edges, so first we remove them. As the system size grows, the reconstruction performance reduces with respect to *FNR* for increasing noise intensity η_0 [Fig. 4(a)], since the noise becomes more dominant than the weak coupling, which prohibits learning $\boldsymbol{H}$ using the coupling effect. As similar to real-world application, *FPR* results are also negligibly small for the noise induced reconstruction case [Fig. 4(b)]. We also performed experiments by generating denser networks where the reconstruction technique fails; therefore, the network sparsity is crucial for the reconstruction (see Supplemental Material [25], Sec. X).

Prediction of emergent behavior.—Although we recover the true network structure, the reduction theory approximates the isolated dynamics $\boldsymbol{f}$ and coupling function $\boldsymbol{H}$ with small bounded fluctuations. As the local dynamics is chaotic and we consider possible noise effect, time evolution forecasting of the given system can diverge from the

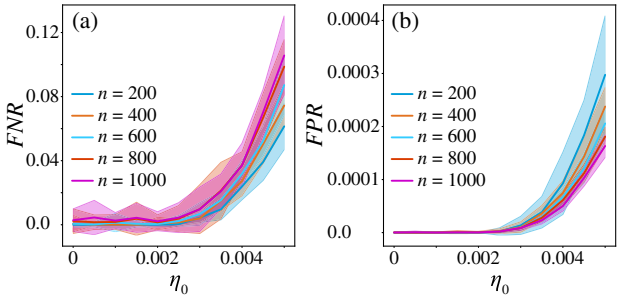

FIG. 4. Average noise effect on reconstruction performance illustrated using (a) *FNR* and (b) *FPR* for 50 realizations of simulations using random scale-free networks of system sizes $n = 200$, 400, 600, 800, and 1000. Time series length is fixed as 500 during all the simulations. The shaded regions represent the corresponding standard deviations.

original system. However, as we recovered the network dynamics with high accuracy for the given data as

$$\boldsymbol{X}(t+1) = \boldsymbol{F}[\boldsymbol{X}(t)] + \gamma \boldsymbol{G}\boldsymbol{X}(t), \tag{4}$$

where γ is the coupling control parameter and initially it is $\gamma = 1$ for the reconstructed model. Then, it is possible to detect critical coupling strength factor γ_c to predict the emergent behavior of the dynamical network by fully analytical techniques if the reconstructed coupling function is identity matrix [47]. For general coupling functions, master stability function [48] or connection graph method [49] can be performed for the detection (see Supplemental Material [25], Sec. XIII).

Conclusions.—The network is fully recovered by our approach in the setting where $\boldsymbol{f}$ is chaotic, the network is scale-free, and the coupling is weak. Because of the weak coupling between nodes and the chaotic nature of the local dynamics, the correlation between measured time series decays exponentially; therefore, it is impossible to reconstruct such complex systems by conventional methods. Cutting-edge autonomous statistical learning techniques also fail when the network size is large. The key idea in our procedure is splitting the model equation into parts by reduction theorem and inferring each unknown ($\boldsymbol{f}$, $\boldsymbol{H}$, and $\boldsymbol{W}$) one by one using sparse recovery. Although the reduction theorem is not established for the general chaotic discrete maps, we showed its validity on various maps. Our approach guarantees the full reconstruction for the noise-free case and small noise intensity even for relatively short time series with no limitations on the network size. However, the quality of reconstruction decreases for increasing noise and the destructive effect of the noise also increases with increasing system size. Finally, obtaining the network dynamics allows one to predict the emergent behavior under parameter changes. There are available regression-based approaches that can learn network topology using short time series [8]; however, it is impossible to detect the critical transitions with only the connectivity. The ability to detect such transitions is crucial for applications such as a transition to collective behavior in the brain network, which can lead to undesired implications. Thus, it is desirable to put forward precautionary norms to avert potential disasters.

Data and code availability.—The data we used in this study can be regenerated by running the code, which is publicly available on GitHub [50].

We are indebted to Tiago Pereira, Matteo Tanzi, Sajjad Bakrani, Arash Rezaeinazhad, Thomas Peron, and Jeroen Lamb for enlightening discussions. This work was supported by The Scientific and Technological Research Council of Turkey (TÜBİTAK) under Grant No. 118C236. D. E. acknowledges support from the BAGEP Award of the Science Academy.

*Corresponding author.
irem.topal@khas.edu.tr
†Corresponding author.
deniz.eroglu@khas.edu.tr

[1] K. Schindler, H. Leung, C. E. Elger, and K. Lehnertz, Brain **130**, e65 (2007).
[2] D. Eroglu, M. Tanzi, S. van Strien, and T. Pereira, Phys. Rev. X **10**, 021047 (2020).
[3] T.-T. Gao and G. Yan, Nat. Comput. Sci **2**, 160 (2022).
[4] W.-X. Wang, Y.-C. Lai, and C. Grebogi, Phys. Rep. **644**, 1 (2016).
[5] M. Nitzan, J. Casadiego, and M. Timme, Sci. Adv. **3**, e1600396 (2017).
[6] T. Stankovski, T. Pereira, P. V. E. McClintock, and A. Stefanovska, Rev. Mod. Phys. **89**, 045001 (2017).
[7] M. Timme and J. Casadiego, J. Phys. A **47**, 343001 (2014).
[8] J. Casadiego, M. Nitzan, S. Hallerberg, and M. Timme, Nat. Commun. **8**, 1 (2017).
[9] T. S. Gardner, D. D. Bernardo, D. Lorenz, and J. J. Collins, Science **301**, 102 (2003).
[10] M. Timme, Phys. Rev. Lett. **98**, 224101 (2007).
[11] S. G. Shandilya and M. Timme, New J. Phys. **13**, 013004 (2011).
[12] D. Yu, M. Righero, and L. Kocarev, Phys. Rev. Lett. **97**, 188701 (2006).
[13] J. Ren, W. X. Wang, B. Li, and Y. C. Lai, Phys. Rev. Lett. **104**, 058701 (2010).
[14] W. X. Wang, R. Yang, Y. C. Lai, V. Kovanis, and M. A. F. Harrison, Europhys. Lett. **94**, 48006 (2011).
[15] W.-X. Wang, Y. C. Lai, C. Grebogi, and J. Ye, Phys. Rev. X **1**, 021021 (2011).
[16] H. Korn and P. Faure, C. R. Biol. **326**, 787 (2003).
[17] A. J. Preyer and R. J. Butera, Phys. Rev. Lett. **95**, 138103 (2005).
[18] G. Werner, Front. Physiol. **1**, 15 (2010).
[19] B. Barzel and A. L. Barabási, Nat. Phys. **9**, 673 (2013).
[20] E. M. Izhikevich, *Dynamical Systems in Neuroscience* (MIT Press, Cambridge, MA, 2007).
[21] F. Dörfler, M. Chertkov, and F. Bullo, Proc. Natl. Acad. Sci. U.S.A. **110**, 2005 (2013).
[22] A. E. Motter, S. A. Myers, M. Anghel, and T. Nishikawa, Nat. Phys. **9**, 191 (2013).
[23] S. Watanabe and S. H. Strogatz, Physica (Amsterdam) **D74**, 197 (1994).
[24] A. T. Winfree, *The Geometry of Biological Time* (Springer Science & Business Media, New York, 2001), Vol. 12.
[25] See Supplemental Material at http://link.aps.org/supplemental/10.1103/PhysRevLett.130.117401, which includes Ref. [26–31], for more examples of network dynamics reconstruction, their sensitivity to network sparsity, and more details on reconstruction algorithm.
[26] W. X. Wang, R. Yang, Y. C. Lai, V. Kovanis, and C. Grebogi, Phys. Rev. Lett. **106**, 154101 (2011).
[27] P. Mehta, M. Bukov, C. H. Wang, A. G. Day, C. Richardson, C. K. Fisher, and D. J. Schwab, Phys. Rep. **810**, 1 (2019).
[28] D. Donoho, IEEE Trans. Inf. Theory **52**, 1289 (2006).
[29] S. L. Brunton and J. N. Kutz, *Data-Driven Science and Engineering: Machine Learning, Dynamical Systems, and*

Control (Cambridge University Press, Cambridge, England, 2019).
[30] L. Huang, Q. Chen, Y.-C. Lai, and L. M. Pecora, Phys. Rev. E **80**, 036204 (2009).
[31] P. Schultz, T. Peron, D. Eroglu, T. Stemler, G. M. Ramírez Ávila, F. A. Rodrigues, and J. Kurths, Phys. Rev. E **93**, 062211 (2016).
[32] T. Pereira, S. van Strien, and M. Tanzi, J. Eur. Math. Soc. **22**, 2183 (2020).
[33] S. L. Brunton, J. L. Proctor, J. N. Kutz, and W. Bialek, Proc. Natl. Acad. Sci. U.S.A. **113**, 3932 (2016).
[34] Y. Y. Liu and A. L. Barabási, Rev. Mod. Phys. **88**, 035006 (2016).
[35] T. Pereira, D. Eroglu, G. B. Bagci, U. Tirnakli, and H. J. Jensen, Phys. Rev. Lett. **110**, 234103 (2013).
[36] R. Tibshirani, J. R. Stat. Soc. Ser. B **58**, 267 (1996).
[37] X. Han, Z. Shen, W. X. Wang, and Z. Di, Phys. Rev. Lett. **114**, 028701 (2015).
[38] E. J. Candes, J. K. Romberg, and T. Tao, Commun. Pure Appl. Math. **59**, 1207 (2006).
[39] M. Novaes, E. R. dos Santos, and T. Pereira, Physica (Amsterdam) **D424**, 132895 (2021).
[40] B. M. de Silva, K. Champion, M. Quade, J.-C. Loiseau, J. N. Kutz, and S. L. Brunton, J. Open Source Software **5**, 2104 (2020).
[41] N. Kasthuri, K. J. Hayworth, D. R. Berger, R. L. Schalek, J. A. Conchello, S. Knowles-Barley, D. Lee, A. Vázquez-Reina, V. Kaynig, T. R. Jones *et al.*, Cell **162**, 648 (2015).
[42] J. T. Vogelstein, E. Perlman, B. Falk, A. Baden, W. G. Roncal, V. Chandrashekhar, F. Collman, S. Seshamani, J. L. Patsolic, K. Lillaney *et al.*, Nat. Methods **15**, 846 (2018).
[43] Q. Wang, G. Chen, and M. Perc, PLoS One **6**, e15851 (2011).
[44] N. F. Rulkov, Phys. Rev. E **65**, 041922 (2002).
[45] N. T. Markov, J. Vezoli, P. Chameau, A. Falchier, R. Quilodran, C. Huissoud, C. Lamy, P. Misery, P. Giroud, S. Ullman *et al.*, J. Comp. Neurol. **522**, 225 (2014).
[46] B. Bollobás, C. Borgs, J. Chayes, and O. Riordan, in *Proceedings of the Fourteenth Annual ACM-SIAM Symposium on Discrete Algorithms* (Society for Industrial and Applied Mathematics, Philadelphia, 2003), SODA '03, pp. 132–139.
[47] D. Eroglu, J. S. Lamb, and T. Pereira, Contemp. Phys. **58**, 207 (2017).
[48] L. M. Pecora and T. L. Carroll, Phys. Rev. Lett. **80**, 2109 (1998).
[49] V. N. Belykh, I. V. Belykh, and M. Hasler, Physica (Amsterdam) **D195**, 159 (2004).
[50] https://github.com/lffrrnt/ReconstructingNetworkDynamics/.